RNA Nanostructures in Physiological Solutions: Multiscale Modeling and Applications

Badu, S. R., Melnik, R., and Prabhakar, S.

**Book Chapter in "Physics of Liquid Matter",
N. Lebovka and L. Bulavin (Eds.), Springer,
O. Physics of Liquid Matter: Modern Problems, Springer
Proceedings in Physics (Book Series), Vol. 171, pp. 337 – 355, 2015.**

Chapter 13
RNA Nanostructures in Physiological Solutions: Multiscale Modeling and Applications

Shyam Badu, Roderick Melnik and Sanjay Prabhakar

Abstract In this review chapter we focus on the nucleic acid nanotechnology research and its application in the biomedical field. We also describe some of our most recent results on the modeling of ribonucleic acid (RNA) nanotubes and their characteristics in physiological solutions. This includes the properties that can be characterised by root mean square deviation (RMSD), radius of gyration and radial distribution function (RDF) for the RNA nanoclusters, paying special attention to RNA nanotubes. We describe the distribution of $^{23}Na^{+}$ and $^{35}Cl^{-}$ ions around the tube as a function of time within a distance of 5 Å from the surface of the tube. The results obtained from our computational studies are compared with available experimental results in the literature. The current developments in the coarse grain modeling of the RNA nanoclusters and other biomolecules are also highlighted.

13.1 Introduction

Extensive studies have been done on nucleic acid nanotechnology research in the biomedical applications. Among others, we recall that the bacteriophage ϕ 29 motor has been constructed to package the deoxyribonucleic acid (DNA) and the X ray crystallography has been used to determine the process of DNA packaging [1]. To construct any kind of nanostructure involving biomolecules the self assembly of small building blocks is very important. One of the notable experimental works has been the development of the crystalline bacterial cell surface using the streptavidin protein [2] which has the tendency of self assembling to construct the building blocks for the nanoclusters that can be used for biomedical applications. The self

S. Badu (✉) · R. Melnik (✉) · S. Prabhakar
MS2 Discovery Interdisciplinary Research Institute, M2NeT Laboratory,
Wilfrid Laurier University, Waterloo, ON N2L 3C5, Canada
e-mail: sbadu@wlu.ca

R. Melnik
e-mail: rmelnik@wlu.ca

L. Bulavin and N. Lebovka (eds.), *Physics of Liquid Matter: Modern Problems*,
Springer Proceedings in Physics 171, DOI 10.1007/978-3-319-20875-6_13

assembly of alkylated peptides can assist in creating the nanobelts in solutions which can be used for various therapeutic applications [3]. Due to the importance of therapeutic applications several kinds of polygon-shaped self assemblies have been developed by using the deoxyribonucleic acid [4–7].

Furthermore, the self assembly of biomolecules, including DNA [8–14], can be used for various bionanodevices in nanobiotechnology. The DNA nanotubes can be used for the alignment of the membrane protein, in order to take the NMR spectrum to determine its crystal structure [15–17]. It has been shown that the stability of the RNA assemblies is higher than that of the DNA self assembled nanoparticles in solutions [18–23]. DNA relaxation under internal viscosity was studied for DNA [24, 25] but no similar study is available for RNA. The thermodynamic stability of any system is determined by calculating its free energy. The system with smaller free energy is more stable, i.e., the RNA has smaller free energy in solutions compared to DNA nanoparticles. The differently shaped structures of the RNA molecules have been formed from the RNA building blocks as well as from their complexes with other biomolecules [26–31].

In the current age of scientific discoveries in nanobiotechnology, the RNA plays a vital role in drug delivery applications. The use of this important molecular system as a drug delivery object to the human body is due to its flexibility in structure. One of the most important building blocks of RNA nanoclusters is the RNAI/II complex. The RNAI and RNAII are defined as the sense and anti sense plasmids that control the replication of COLE1 plasmid [32, 33]. COLE1 is a DNA molecule separated from chromosomal DNA that is found in the cell of bacteria. The sequence for the RNAI is (GGCAACGGAUGGUUCGUUGCC) and the sequence for the RNAII is (GCACCGAACCAUCCGGUGC) [34]. The schematic diagram for the RNAI/II complex is shown is Fig. 13.1. Using these building blocks, the experimental work has been performed to see the varieties of self assemblies of this complex. Experimentally it has been found that there are varieties of self assemblies formed by the end of the experiment. Notably, it has been found that the hexagonal ring is one of the most abundant self assemblies [35] formed during the experiment performed at the solution phase. The formation of the hexagonal nanoring from the pRNA strand has been studied experimentally, and has

Fig. 13.1 Formation of the RNAI/II complex via base pairing between two segments

been later verified theoretically. During the experiment the RNAI/RNAII complex was put into the vessel and let molecules to assemble following the specific experimental protocol. The system was heated at first to the 95 °C for 2 min, then cooled to 4 °C and then warmed to 30 °C and supplied to the buffer solution. Then the system is supplied to the polycrystalamide gel experiment (PAGE) and TGGE experiment using a specific experimental setup which is described in [35].

It has been found that the majority of the assemblies are hexagonal rings with very few assemblies with square and octahedral structures. The low abundance of the tetramer and the pentamer assemblies of the RNAI/II complexes is due to the fact that they are less thermostable. Similar situation has been found in the case of higher order species like septamers and octamers. This result is found to be similar to the results obtained in [36]. An increasing interest to the field of RNA nanoclusters is due to their potential use in the drug delivery, nanodesign, therapy, among other fields. The ribonucleic acid is the polymer containing four kind of nucleobases; adenine, uracil, cytosine and guanine. These four kinds of the nucleobases are connected via sugar ring and the phosphate backbone to form the long chain polymer. A combination of the sugar ring and the nucleobase is known as the nucleotide. The size of the RNA strand is defined by the number of the nucleotides present in the polymer which eventually gives the number of possible structures that can be made from the given set of the nucleotides. The difference between the RNA and the DNA is that the uracil will be replaced by the thymine in DNA. In their double strand structure the stability is well described on the basis of the base pairing between them.

The development of bionanotechnology has facilitated the varieties of the techniques to detect and diagnose the cancer and other diseases. The use of bionanoparticles consisting of the RNA is due to their small size which let them to have assess to most of the parts of the body to interact with the infected or damaged cells. Ultimately, the models for RNA should be coupled with nonlinear dynamics models of cells [37]. In order to make the modeling of RNA nanoclusters successful, it is very important to have the suitable RNA building blocks. The self assemblies of RNA nanoclusters are performed in two ways. One is templated and the other is non-templated. If the self assemblies of RNA building blocks are done by the interaction between them from the external influence then this kind of self assemblies are known as templated, whereas if there is no external influence, during the interaction between the building blocks, then that kind of self assemblies are known as the non-templated self assemblies. Furthermore, the building blocks of nanorings are engineered in such a way that the RNAI and RNAII ends are complementary to each other. The complexation of these two RNA fragments via sticky ends is an important feature for constructing nanoclusters like RNA nanorings and nanotubes. In short, by using six helical building blocks of either one or two types (RNAI/RNAII) the nanoring is formed by self-assembling them via base pairing hydrogen bonds. The structure of the nanoring including the links that are used to form the nanotube is presented in Fig. 13.2. The stability of the nanoring depends on RNAI/RNAII interactions. The design of the sticking ends helps to assemble the nanorings to build the nanotubes. The starting structures of the RNAIi/RNAIIi

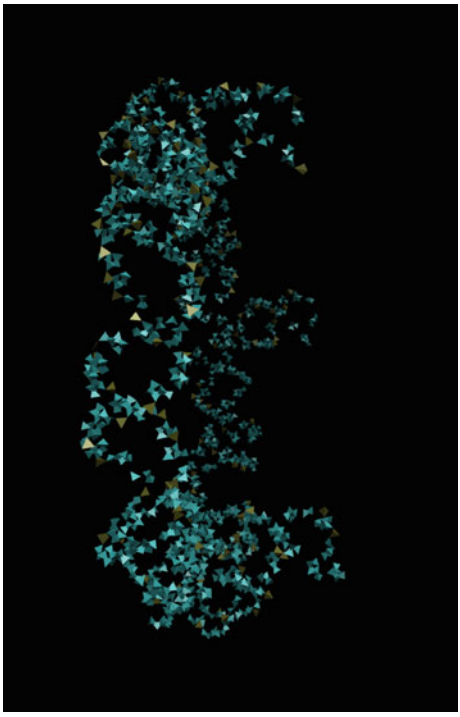

Fig. 13.2 RNA nanoring including three tails to link them to form the RNA nanotube

complex are taken from the protein data bank with the pdb code (2bj2.pdb) [34]. Recently, RNA has been self-assembled to build nanoscale scaffolds [38] using computational techniques and experiments. In the literature it is reported that several forms of RNA motifs can be constructed to provide a proper multifunctional RNA nanocluster; however only a few of them are found to be useful for drug delivery [39]. Assembling should be used to build the RNA nanocluster from the RNA building blocks [40].

RNA has been used to build the higher order self assembly in vitro [41] and in vivo [42] by assembling the multidimensional RNA structures. It has been used for the bacterial metabolism. RNA nanotechnology research is still in progress to achieve complete benefit from it. Furthermore, the RNA molecules can survive at low pH values that makes RNA to be compatible for the drug delivery and therapy in vivo. These RNA molecules can produce the self assemblies in vivo. They are transcribable using the DNA as a template [43–50]. The important factor that needs to be considered during the drug delivery process is the toxicity and the safety issues related to nanomaterials used for this process [51, 52].

There are two possible ways to deliver therapeutic drugs into the human body. Firstly, it can be done by directly including it into the RNA building blocks. Secondly, it can be done by attaching the drug at some particular ends of the RNA nanotube. The RNA nanotube can be useful for many applications, in particular for the delivery of drugs into the human body due to its stable condition at all

temperatures as experiments show [53]. The target delivery vehicle, i.e. the RNA nanoclusters built for the drug delivery, should be stable, so that the modeling of such kinds of structures is critical. We note that the hairpin-like structure of the nanocluster has already been modeled [54] from RNA interference polymers. The discovery of a small interfering RNA (siRNA) [55, 56] is one of the most important research achievements in this field. The siRNA is basically a synthetic double stranded RNA with 21 basepairs. The function of siRNA is to suppress the problematic genes by RNA interference [57]. It also can be used for safe and efficient delivery of siRNA to cells. The use of the small interfering RNA is somewhat incomplete until its safe way of the delivery to the human body is determined. For this purpose the DNA packaging of bacteriophase ϕ 29 has been modified and used to package the siRNA for safe delivery to the human body [58, 59]. The delivery of oligonucleotides has also been studied to understand the effectiveness of models of the cancer therapy in humans [60]. The RNA molecules of the size with 18–30 nucleotides are also important in regulating the gene expression in the cytoplasm and nucleus [58, 61–63].

Previously, our group [64, 65] studied the mechanical and thermodynamical properties of RNA nanorings [36] using the molecular dynamics technique, and such studies on the RNA nanotubes have also been under way. The results obtained for the nanoring were later supported by experimental results using biochemical and biophysical techniques [35]. Specifically, the issues addressed in the previous papers have been the stability of the nanoring versus temperature, effect of the environment (i.e. solvent and counteractions) on its stability, as well as the conformations and dynamics under external forces. Some anomalous behaviour has been observed with the variation of temperature of the simulation box containing the nanoring. In a recent study, the properties of human immunodeficiency virus on hairpin-like subtype-A and subtype-B at different salt concentrations and magnesium bindings have been explored using molecular dynamics techniques [66]. Also an experimental study of the concentration dependence of NaCl and KCl on the free energy of RNA hairpin folding has been done [67]. Such studies provide additional motivations to do the molecular dynamics simulations of RNA nanoclusters. Furthermore, the first coarse-grained model for RNA nanorings has been developed [68] by utilizing the molecular dynamics simulations method.

13.2 Molecular Dynamics Simulation of Biomolecules

Molecular dynamics simulation involving biomolecules has become very important to understand the dynamics of biological systems. Specifically, the molecular dynamics simulation gives the idea about the dynamic behaviour of the biomolecules in physiological solutions, it gives the average of the thermal properties of the biomolecules under study and prediction of the thermally compatible conformation of the molecules [69, 70]. Theoretical basis of the molecular dynamics lies with statistical thermodynamics models and solving the Newton's equations of motion of

the many particle system involving atoms. Recently, several molecular dynamics studies have been done on the RNA molecules and their derivatives [71–73]. Some of the most important structures derived from RNA molecules are the RNA hairpin loops for which the molecular dynamics simulation has been performed to calculate potential of mean force as a function of distance between two ends of the loop. The stability of the hairpin loops has been calculated and compared to the experimental results which were found to be in close agreement [73]. Furthermore, the molecular dynamics simulation has been performed on the viral RNA dependent polymers to understand their function and structure [72]. In our group the molecular dynamics simulation has been done on the varieties of the RNA nanoclusters. Some of the most recent results related to the RNA nanoclusters [64, 65] will be briefly presented in the following sections.

13.3 Multiscale Modeling

In multiscale modeling calculation of the properties of the system at one level is done using the models from a different level. There are a number of multiscale modeling methodologies used in applications. Here we describe three of them, typical for biological applications [74–77], namely:

1. The Boltzmann inversion method
2. The force matching method for developing the coarse-grained modeling
3. Multiscale coupling method for direct transfer of the information from mesoscopic and atomic scales during the simulation.

The first method commonly used in the multiscale modeling is the Boltzmann inversion method which has also been used in the coarse-grained modeling of the RNA nanoclusters. This will be discussed in details in the following section.

In the force matching process [78], the objective function, depending upon the parameter α, is defined follows

$$Z(\alpha) = Z_F(\alpha) + Z_c(\alpha), \tag{13.1}$$

$$Z_F(\alpha) = \left(3\sum_{k=1}^{M} N_k\right)^{-1} \sum_{k=1}^{M}\sum_{i=1}^{N_k} |F_{ki}(\alpha) - F_{ki}^0|^2, \tag{13.2}$$

$$Z_C(\alpha) = \sum_{r=1}^{N_C} W_r |A_r(\alpha) - A_r^0|^2. \tag{13.3}$$

The integer M in Z_F (the force objective function) is the number of configurations, N_k is the number of atoms in the kth configuration and $F_{ki}(\alpha)$ is the force on the ith atom in the kth configuration which is obtained from the parametrization of α, and the F_{ki}^0 is the corresponding reference force obtained from the first principles

calculations. In the constraint objective function Z_C the quantities $A_r(\alpha)$ are also physical parameters obtained from parametrization, A_r^0 are experimental values or the values calculated from the first principles methods and W_r is the weight factor. The force objective function defined in (13.1) is minimized for given α to calculate the classical force parameters by using the force and physical quantities obtained from ab initio calculations. Therefore, in order to calculate the force objective function, and constraint objective function it is necessary to do the ab initio calculations. The parameters α defined in the above (13.1, 13.2, 13.3) are calculated by matching the forces obtained by using the first-principles calculations of the several configurations of the molecular system and the classical potentials [78–80].

At the mesoscopic level, there exist effective field theories to apply the continuum mechanics. Also there are particle-based methodologies that have been developed to give more accurate results in the study than it is possible to deduce from the mesoscopic scale. Further details on particle-based methods can be found in [81–83].

13.4 Developments in Coarse-Grained Modeling of RNAs

Although due to the current development of the computational techniques and feasible computational resources, the theoretical study of the bimolecular systems has become much easier, preserving the physical information of the molecular system in the model remains very crucial. In view of this, the coarse-grained models are designed to explain information about the system at larger scales from the smaller scale that are modeled from the atomistic classical approach. The developed coarse-grained models should be easy enough to simulate accurately enough the physical characteristics of the system. In the coarse-grained modeling we represent the sum of atoms as a pseudo atom and then define an effective energy function U_{CG} that determines the thermodynamical properties, which should be identical to the system's properties once the proper energy function is predicted. Using coarse-grained models, the research has been done to study the structural and physical properties of DNA [84]. There are many other DNA studies found in the literature to describe the six helical systems [85] using atomic force microscopy. Also the study has been done for the improved angle potential [86]. In this study the array of hexagonal six helix bundles are described in 1D and 2D cases. Furthermore, several studies [87–89] of other bimolecular systems using the coarse-grained modeling have been done. Recently, the modeling of the coarse-grained structure of RNA and RNA-Protein using the fluctuation matching method has been performed [90], in which the authors also followed the assumptions used in [68]. There are a number of other investigations done on coarse grained modeling of RNA for the prediction of the tertiary structures [91–94]. In one of the earlier studies on the coarse-grained modeling of the RNA 3D structure, a single nucleobase has been approximated by five pseudo atoms [95]. In order to determine the forcefield parameters the 688 experimentally determined structures of

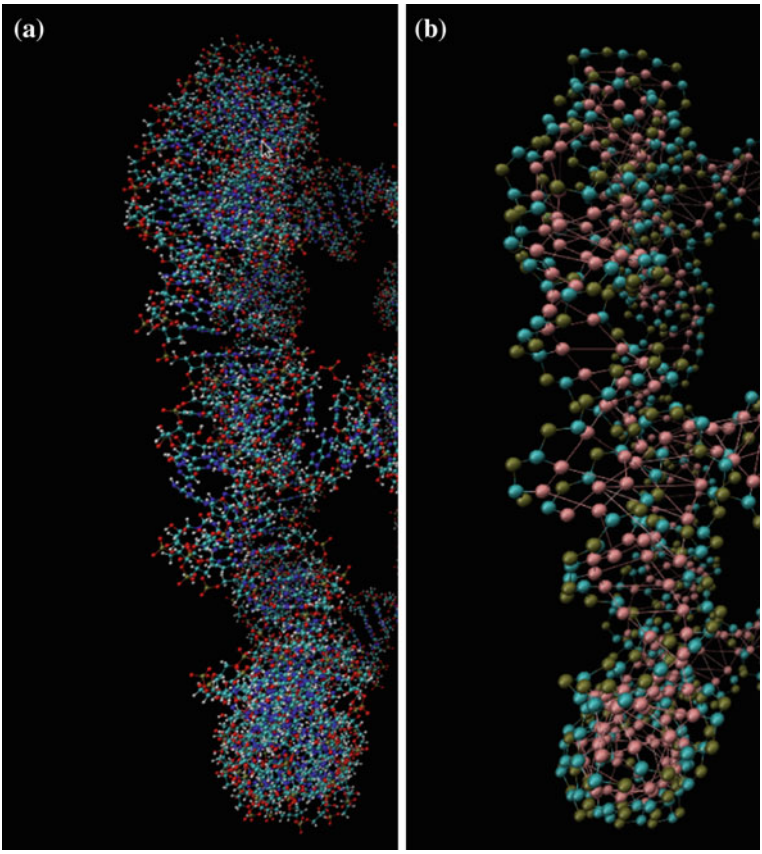

Fig. 13.3 **a** Part of the RNA nanocluster in all atom representation. **b** Part of the RNA nanocluster in coarse grained representation

RNA have been used. The transformation of the all atom model to the coarse-grained model in our typical three bead approximation is demonstrated in Fig. 13.3 where a part of the RNA nanoring is presented in both all atom and coarse-grained representations.

13.5 Computational Details

In molecular dynamics simulation the classical equations of motion of a molecular system are solved by their time dependent integration. The potential of the system used during the molecular dynamics simulation using CHARMM force field can be expressed as follows.

$$V_{total} = \sum_{bond} K_b(r - r_0)^2 + \sum_{angle} K_\theta(\theta - \theta_0)^2 + \sum_{dihedral} K_\phi(1 + cos(n\phi - \gamma)) + \sum_{Hbond} \left(\frac{C_{ij}}{r_{ij}^{12}} - \frac{D_{ij}}{r_{ij}^{10}}\right) + \sum_{impropers} K_w(w - w_0)^2 + \sum_{Urey-Bradley} K_u(u - u_0)^2 + \sum_{Vanderwaals} \left(\frac{A_{ij}}{r_{ij}^{12}} - \frac{B_{ij}}{r_{ij}^{10}}\right) + \sum \frac{q_i q_j}{\varepsilon r_{ij}}. \quad (13.4)$$

In (13.4), the first term corresponds to bonds, second corresponding to angle parameters, the third term corresponds to the potential energy and interactions arised from the dihedral angles in the molecular system, the fourth term defines the interaction coming from the hydrogen bonds which includes the base pairing as well as the hydrogen bonding between the RNA and the water molecules. The fifth term known as the improper term that arised due to out-of-plane bending of molecular system and the sixth term is the Urey-Bradley contribution. The improper term is included in the potential energy expression to maintain the planarity of the molecule. Finally, the last term in the potential expression represents the long distance interactions known as the van der Waals' interactions. We have performed all-atom molecular dynamics simulations of RNA nanotubes by using the CHARMM27 force field [96] implemented in the NAMD package [97] as it was done for the nanoring [64, 65].

The CHARMM is the force field widely used for the molecular dynamics simulation that is implemented in several molecular dynamics packages like LAMMP, NAMD and GROMACS. The CHARMM27 force field is one of the most important force fields which is developed for the nucleic acid through the empirical force field determinations. This is the most recent force field which is obtained from the reoptimization of the earlier force field CHARMM22 [97–99]. During the optimization of the force field the importance is given to the balancing of the properties of the local small molecules to the global system. In the studies [98, 99] the development of the CHARMM force field was carried out and its compatibility for the DNA and the RNA has been tested. It was found that the results are close to the experimental results.

The modeling of the nanotube, visualization and the analysis of the simulation outputs have been performed using the software visual molecular dynamics (VMD) [100]. The VMD is a molecular graphics software developed to display the biomolecular systems like biopolymers and proteins interactively. In this program the molecules can be viewed in several colors and several kind of representations. This can allow us to modify a particular protein structure as needed. In particular, one can do mutation, delation or addition of bonds between the atoms using VMD tool. Furthermore, we can display several structures at the same time using VMD. The trajectory of the molecular dynamics simulation can be displayed as well as analysed to study the molecular properties. The VMD program is written in C++

and is provided with the complete documentation with instructions to use it. This program is compatible with several kinds of molecular dynamics simulation packages including NAMD, LAMMP, GROMACS etc.

In our typical runs, the RNA-nanotube has been solvated in a water box. The size of the box is taken in such a way that the distance from the surface of the nanocluster to the wall is slightly larger than the cut off radius used in the molecular dynamics simulation. In order to make the system neutral we have added 924, and 1254 $^{23}Na^{+}$ ions for three ring and four ring nanotubes, respectively. Furthermore, to make the solution equivalent to physiological solutions we have added extra 924 and 1254 $^{23}Na^{+}$ and $^{35}Cl^{-}$ ions to the three ring and four ring nanotube, respectively. The resulting system has been first simulated at constant temperature and pressure using the NAMD software package. The temperature in the system has been controlled by using Langevin's method with damping $\eta = 5\ ps^{-1}$. For adding chemical bonds between the segments in the nanoclusters we have used the topotools available in the VMD.

13.6 Results and Discussions

Advancing further multiscale models for RNA nanoclusters, we have modeled the RNA nanotubes with multiple nanorings. Some of the most recent results have been presented in our papers [65, 101]. For the modeling of RNA nanotubes the hexagonal nanorings were connected to each other by using the links between them as described in our earlier studies [64, 65, 101]. Typical sample structures of the three ring nanotube without water and with water are presented in Fig. 13.4a, b respectively. The six helical segments are constructed from RNAI and RNAII building blocks. Also, the tails used to connect the RNA nanorings are the double strand RNAs with the length of 22 nucleotides.

As we discussed earlier, the RNAIi and RNAIIi are the double strand RNAs. By using the VMD tools we were able to connect multiple rings via three links at junctions presented in Fig. 13.4b. The links used in connecting the multiple numbers of nanorings (to build the RNA nanotube) are composed of helical double strand RNAs with 22 nucleobases. Three links are used in between two consecutive rings to connect them to form the nanotubes as shown in Fig. 13.4b. The chemical bonds between the ring and the links are mediated through the phosphorous of the phosphate group in the ring and the oxygen in the sugar ring of the corresponding link or vice versa. Using NAMD, we optimized the chemical bonds added between different segments of the RNA nanoclusters.

Here at first, we present the results for the RNA nanotube of different sizes obtained from the molecular dynamics simulation. The results for the simulation of three the ring nanotube are summarized in Figs. 13.5 and 13.6. Figure 13.5 describes the variation of the energy and temperature as a function of simulation time. At the beginning of the simulation the energy of the system varies and then becomes stable once the system becomes stabilized. Here in our results we have presented only the latter part of the simulation, which is also known as the

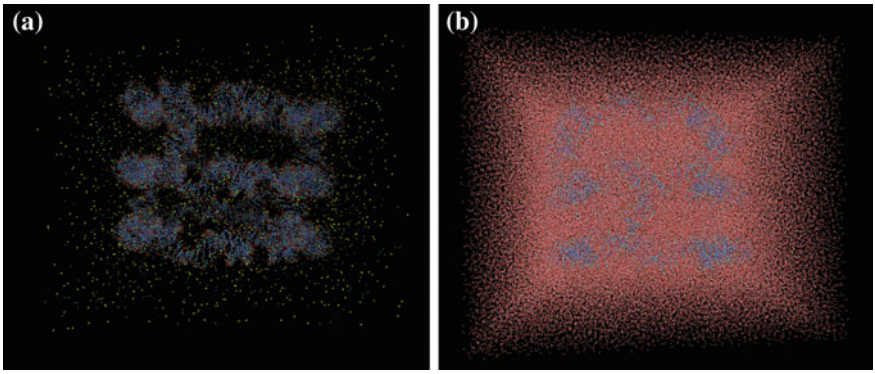

Fig. 13.4 **a** Three ring RNA nanotube and ions without water and **b** three ring RNA nanotube in a physiological solution

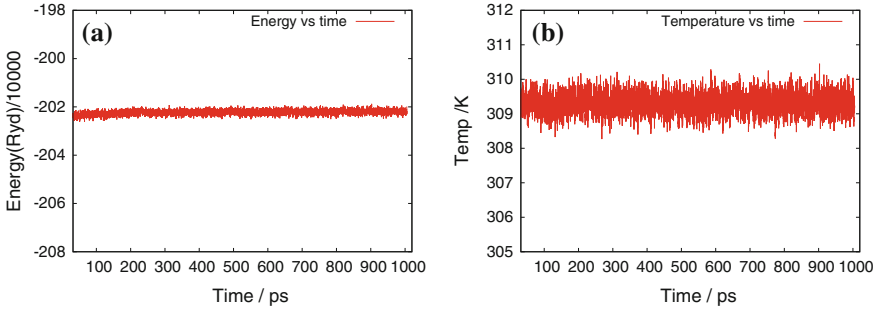

Fig. 13.5 **a** Energy and **b** temperature versus simulation time for the all-atom molecular dynamics simulation of three ring RNA nanotube in water and salt

production region of simulation. All our results and analysis of the properties are presented from this production region of molecular dynamics simulation. The temperature of the system remains almost stable with some fluctuations. In Fig. 13.6 we present the calculated properties such as the number of ions around the RNA nanotube within the distance of 5 Å at different temperatures, the number of bonds per basepairs, the radius of gyration and the root mean square deviation at two temperatures, 310 and 510 K. The results corresponding to variations of the parameters are similar to the results obtained for the other nanoclusters described in our earlier studies [64, 65, 101].

The nature of the radial distribution function plots calculated for the three ring RNA nanotube is revealed in Fig. 13.7. In particular, four subplots in this figure present the RDF plots for phosphorous-phosphorous, phosphorous-water, phosphorous-sodium and phosphorous-chlorine, respectively. From the P–P RDF plots presented in Fig. 13.7a, we see that there are three well-pronounced peaks around the same positions at it was observed for other nanoclusters studied in our

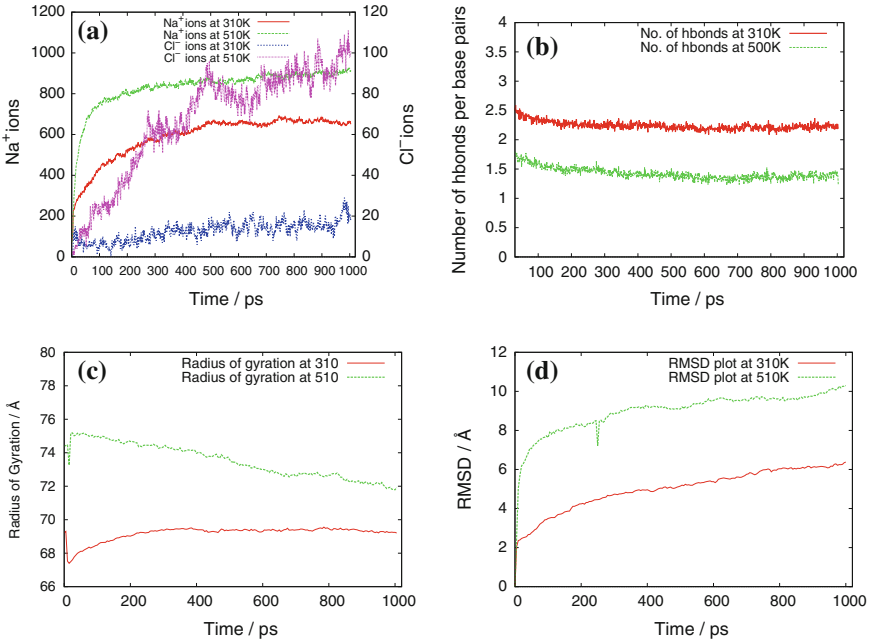

Fig. 13.6 **a** Number of ions with the range of 5 Å. **b** Number of bonds per base pairs. **c** Radius of gyration and **d** RMSD of three ring RNA nanotube obtained from all atom molecular dynamics simulation

paper [65]. These peaks actually show the first, second and third nearest neighbours of the phosphorous atom respectively. The intensity of the peaks is increased on going from 310 to 510 K. The position of the first peak is at the same position, whereas the second and third peaks are shifted slightly to the lower distances at 510 K in comparison to their positions at 310 K.

From the P–OH2 RDF plots presented in Fig. 13.7b calculated at temperatures 310 and 510 K, it is clear that for each RDF there is a peak around the distance of 4 Å. This first peak indicates the first solvation shell around the phosphorous atom taken from the surface of the RNA nanotube. Similarly, the second small peak shows the second solvation peak for the phosphorous atom in the phosphate backbone of RNA strands that builds the RNA nanotubes. In the rest of the range, the nature of the P–OH2 RDF plots remained more or less stable showing that the water molecules are distributed uniformly after certain distance from the surface of the RNA nanotube. In spite of showing a similar trend at both temperatures, the height of the first peak is significantly dropped on going from 310 to 510 K. This indicates that a significant amount of water molecules are expelled out from the surface of the RNA nanocluster at higher temperatures as demonstrated in our earlier papers [64, 65].

The P–Na RDF plots for the three ring RNA nanotube at both temperatures are presented in Fig. 13.7c. The RDF plot for P–Na shows the first peak at around 3.5 Å

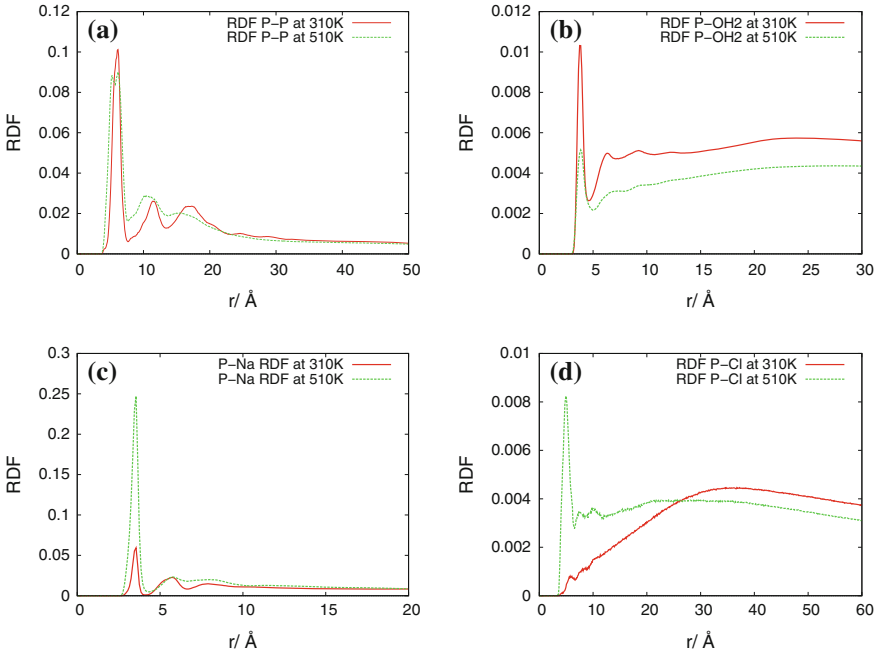

Fig. 13.7 Radial distribution function for three ring RNA nanotube. **a** P–P. **b** P–OH2. **c** P–Na. **d** P–Cl

at both temperatures, 310 and 510 K. This shows that most of the sodium ions are around this distance at the final step of all-atom molecular dynamics simulation. One significant difference between the RDF plots at 310 and 510 K is that the first peak of the radial distribution function is significantly increased on going from 310 to 510 K. This feature supports the conclusion that we made from the ionic distribution plots presented in Fig. 13.6a. Furthermore, the P–Cl RDF plots presented in Fig. 13.6d show that the chloride ions are far away from the surface of the RNA nanotube at 310 K. When the temperature of the system is increased from 310 to 510 K the $^{35}Cl^{-}$ ions are also aggregated significantly closer to the surface of the RNA nanotube as observed from the first peak of RDF plot at 510 K. The height of the peak at a particular distance from the surface of RNA nanotube in the RDF plot is proportional to the number of $^{35}Cl^{-}$ ions at that distance. This means that the number of $^{35}Cl^{-}$ ions around the first peak at 510 K are larger in comparison to the number of $^{35}Cl^{-}$ ions at 310 K as observed from the plots for the number of $^{35}Cl^{-}$ ions at 310 and 510 K presented in Fig. 13.6a.

The results for the four ring RNA nanotube are presented in Figs. 13.8, 13.9 and 13.10. The nature of solvation and the ionic distribution during the molecular dynamics simulation have been found to be similar to those found in the case of the three ring nanotube as well as to the results described in our earlier work [64, 65]. For all of these systems we see that the peaks for the P–P RDF remain almost the

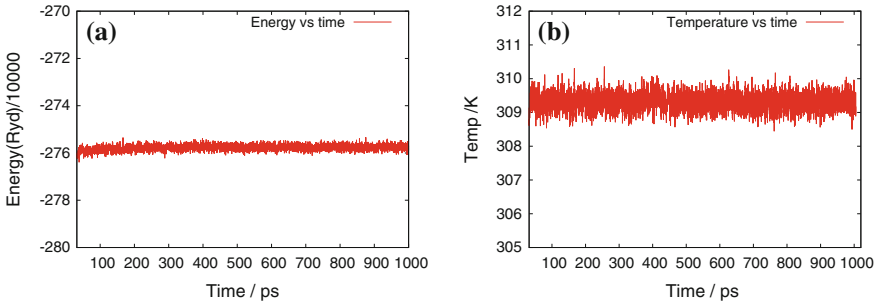

Fig. 13.8 **a** Energy and **b** temperature versus simulation time for the all-atom molecular dynamics simulation of four ring RNA nanotube in water and salt

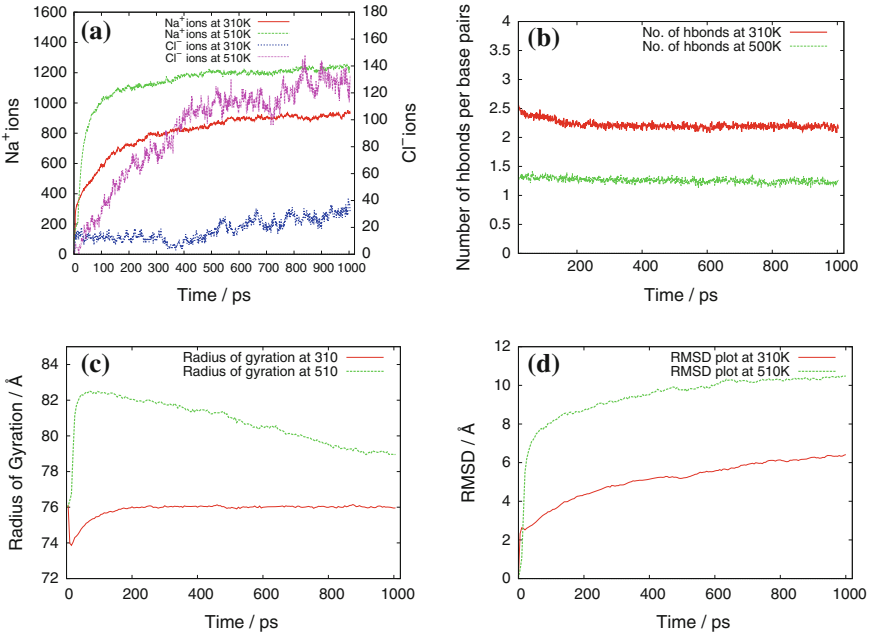

Fig. 13.9 **a** Number of ions with the range of 5 Å. **b** Number of bonds per base pairs. **c** Radius of gyration and **d** RMSD of four ring RNA nanotube obtained from all atom molecular dynamics simulation

same, for P–OH2 the intensity at the peak is decreased on increasing the temperature, but in the P–Na and P–Cl RDF plots the intensity of the first peaks is significantly increased on going from 310 to 510 K temperature. From these observations we can conclude that the $^{23}Na^{+}$ and $^{35}Cl^{-}$ ions are attracted toward the surface of the nanocluster and the water molecules are pushed away from the surface as the temperature is increased. In short, we observe that the ions are being

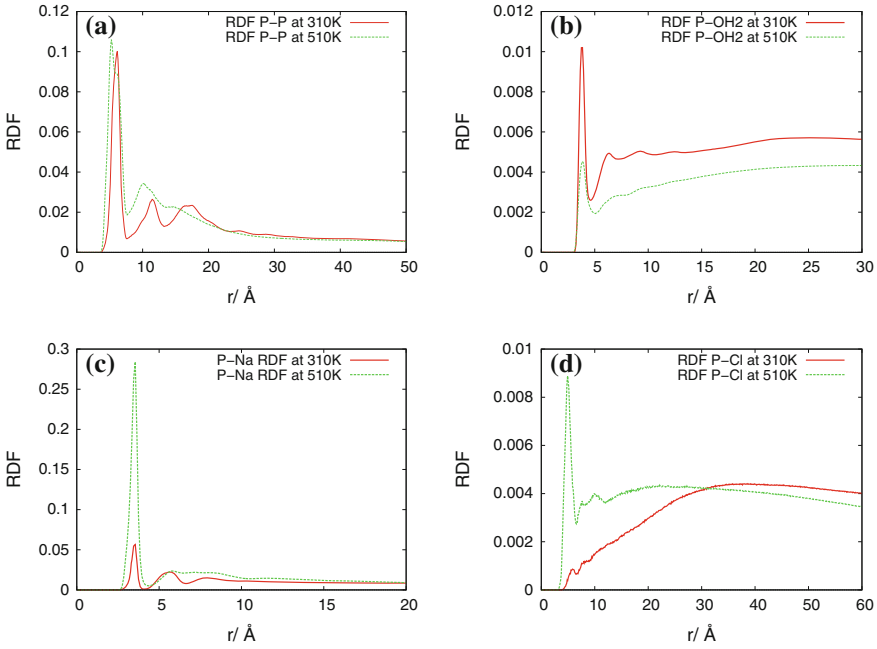

Fig. 13.10 Radial distribution function for four ring RNA nanotube. **a** P–P. b P–OH2. **c** P–Na. **d** P–Cl

precipitated around the surface of the RNA nanocluster as the temperature of the system is increased. This phenomenon of self stabilization was first discovered in [64] and has recently been observed for a larger class of RNA nanoclusters in our earlier work [65].

In spite of existing difficulties in the modeling of the nanostructures from the building blocks consisting of nucleic acids and their derivatives structures, significant achievements have been observed in the field of RNA nanotechnology. Clearly, there is a scope for further improvements. Notably that although there are several state-of-the-art computational software packages developed to predict RNA nanostructures, only 70 % accuracy has been found in the prediction and folding of the RNA nanoclusters [102, 103].

13.7 Conclusions

In this chapter we have reviewed some of the aspects of the nucleic acid research and their potential applications in nanobiomedicine and other related fields. From the review of the literature, we conclude that the RNA is more versatile and compatible for the biomedical applications in the human body, compared to other

alternatives, due to its flexibility in structure as well as the absence of toxicity issues to be addressed. In view of this, we have studied the structure and properties of RNA self assemblies in physiological solutions. In our earlier investigations [64, 65], the analysis of the physical properties of the nanoring has been reported. The RNA nanoring is a small system in comparison to the nanotube and has limited practical applications in bionanotechnology. However, it provides an excellent testing ground for further studies. In our most recent studies [65, 101]. This included the optimized structures of nanotubes up to the size of 40 nm have been analyzed for the first time. The individual RNA nanorings were connected via double-helical rings mediated by the bonds between the phosphate group and sugar ring. The newly added bond lengths have been optimized by using algorithms available in NAMD. Then, starting from nanorings, the results for the RNA-nanotubes of different sizes have been exemplified in this chapter for three and four nanoring structures and discussed in details. Similar to our earlier study [65] we presented some of the results for these RNA nanotube structures via calculations of the root mean square deviation, radius of gyration, number of hydrogen bonds per basepair, ion accumulation around the tube, and the radial distribution functions. From our present analysis it is clear that the quality of the results are likely to be improved further by doing the molecular dynamics simulation for longer time ranges. Another way to improve the quality of the results lies with further developing of the multiscale models methodologies specifically for these structures e.g. coarse-grained modeling methods that would allow one to perform molecular dynamics simulations for longer ranges of time, closer to the time scales of real biological phenomena. These kinds of developments are currently under way in our lab. Furthermore, these new developments will help further progress in theoretical bionanotechnology, as well as guide the experimentalists working in this filed. Also, the use of reduced order modeling [104] would increase the compatibility of the results with the time range better comparable to real biological processes. So far we have been using the SHARCNET parallel computing facilities for calculating of the properties of the RNA nanoclusters using the 64 processors for each simulation. Using the clusters such as GPGPUs or Phi co-processors may make these computations more efficient for larger RNA nanoclusters as well as for longer time ranges. For drug delivery applications computational efforts will also be dependent on the shape of the nanocluster as well as on the drug particle to be delivered [105]. In our modeling of the RNA nanoclusters, we have control on the size of the nanocluster which gives better potentiality of their use in the nanomedicine.

Our progress in the development of RNA nanoclusters will boost further their applications in the therapy, nanodesign and drug delivery, among other fields.

Acknowledgments Authors are grateful to the NSERC and CRC Programs for their support and Shared Hierarchical Academic Research Computing Network (SHARCNET: www.sharcnet.ca) for providing the computational facilities. Finally, we would like to thank Dr. P.J. Douglas Roberts for helping with technical SHARCNET computational aspects.

References

1. A.A. Simpson, Y. Tao, P.G. Leiman, M.O. Badasso, Y. He, P.J. Jardine, N.H. Olson, M.C. Morais, S. Grimes, D.L. Anderson, T.S. Baker, M.G. Rossmann, Nature **408**(6813), 745 (2000)
2. D. Moll, C. Huber, B. Schlegel, D. Pum, U.B. Sleytr, M. Sra, PNAS **99**(23), 14646 (2002)
3. H. Cui, T. Muraoka, A.G. Cheetham, S.I. Stupp, Nano Lett. **9**(3), 945 (2009)
4. D. Liu, M. Wang, Z. Deng, R. Walulu, C. Mao, J. Am. Chem. Soc. **126**(8), 2324 (2004)
5. F.A. Aldaye, H.F. Sleiman, J. Am. Chem. Soc. **129**(44), 13376 (2007)
6. P.W.K. Rothemund, N. Papadakis, E. Winfree, PLoS Biol. **2**(12), e424 (2004)
7. S.H. Park, R. Barish, H. Li, J.H. Reif, G. Finkelstein, H. Yan, T.H. LaBean, Nano Lett. **5**(4), 693 (2005)
8. T.P.J. Knowles, T.W. Oppenheim, A.K. Buell, D.Y. Chirgadze, M.E. Welland, Nat. Nanotechnol. **5**(3), 204 (2010)
9. N.C. Seeman, Annu. Rev. Biochem. **79**, 65 (2010)
10. C. Lin, Y. Liu, H. Yan, Biochemistry **48**(8), 1663 (2009)
11. F.A. Aldaye, A.L. Palmer, H.F. Sleiman, Science **321**(5897), 1795 (2008)
12. K. Tanaka, A. Tengeiji, T. Kato, N. Toyama, M. Shionoya, Science **299**(5610), 1212 (2003)
13. M. Endo, T. Sugita, Y. Katsuda, K. Hidaka, H. Sugiyama, Chem. Eur. J. **16**(18), 5362 (2010)
14. Y. Ke, S. Lindsay, Y. Chang, Y. Liu, H. Yan, Science **319**(5860), 180 (2008)
15. B. Yurke, A.J. Turberfield, A.P. Mills, F.C. Simmel, J.L. Neumann, Nature **406**(6796), 605 (2000)
16. S.M. Douglas, J.J. Chou, W.M. Shih, PNAS **104**(16), 6644 (2007)
17. M. Endo, N.C. Seeman, T. Majima, Angew. Chem. Int. Ed. **44**(37), 6074 (2005)
18. N. Sugimoto, S.I. Nakano, M. Katoh, A. Matsumura, H. Nakamuta, T. Ohmichi, M. Yoneyama, M. Sasaki, Biochemistry **34**(35), 11211 (1995)
19. A. Kitamura, P.J. Jardine, D.L. Anderson, S. Grimes, H. Matsuo, Nucl. Acids Res. **36**(3), 839 (2008)
20. P. Guo, Nat. Nano. **5**(12), 833 (2010)
21. W.W. Grabow, L. Jaeger, Acc. Chem. Res. **47**(6), 1871 (2014)
22. M.S. Searle, D.H. Williams, Nucl. Acids Res. **21**(9), 2051 (1993)
23. K.A. Afonin, W. Kasprzak, E. Bindewald, P.S. Puppala, A.R. Diehl, K.T. Hall, T.J. Kim, M.T. Zimmermann, R.L. Jernigan, L. Jaeger, B.A. Shapiro, Methods **67**(2), 256 (2014)
24. J. Yang, R. Melnik, Discrete and continuous dynamical systems, supplement pp. 1052–1060 (2007)
25. X. Yang, R. Melnik, Comput. Biol. Chem. **31**, 110 (2007)
26. M. Anokhina, S. Bessonov, Z. Miao, E. Westhof, K. Hartmuth, R. Lührmann, EMBO J. **32** (21), 2804 (2013)
27. I. Severcan, C. Geary, E. Verzemnieks, A. Chworos, L. Jaeger, Nano Lett. **9**(3), 1270 (2009)
28. I. Severcan, C. Geary, A. Chworos, N. Voss, E. Jacovetty, L. Jaeger, Nat. Chem. **2**(9), 772 (2010)
29. E. Osada, Y. Suzuki, K. Hidaka, H. Ohno, H. Sugiyama, M. Endo, H. Saito, ACS Nano **8**(8), 8130 (2014)
30. L. Jaeger, A. Chworos, Curr. Opin. Struct. Biol. **16**(4), 531 (2006)
31. N.B. Leontis, E. Westhof, Science **345**(6198), 732 (2014)
32. J.I. Tomizawa, Cell **38**(3), 861 (1984)
33. J.I. Tomizawa, Cell **47**(1), 89 (1986)
34. A.J. Lee, D.M. Crothers, Structure **6**(8), 993 (1998)
35. W.W. Grabow, P. Zakrevsky, K.A. Afonin, A. Chworos, B.A. Shapiro, L. Jaeger, Nano Lett. **11**(2), 878 (2011)
36. Y.G. Yingling, B.A. Shapiro, Nano Lett. **7**(8), 2328 (2007)
37. R.V.N. Melnik, X. Wei, G. MorenoHagelsieb, J. Biol. Syst. **17**(03), 425 (2009)

38. K.A. Afonin, E. Bindewald, A.J. Yaghoubian, N. Voss, E. Jacovetty, B.A. Shapiro, L. Jaeger, Nat. Nanotechnol. **5**(9), 676 (2010)
39. N.B. Leontis, A. Lescoute, E. Westhof, Curr. Opin. Struct. Biol. **16**(3), 279 (2006)
40. D. Shu, Y. Shu, F. Haque, S. Abdelmawla, P. Guo, Nat. Nanotechnol. **6**(10), 658 (2011)
41. B. Cayrol, C. Nogues, A. Dawid, I. Sagi, P. Silberzan, H. Isambert, J. Am. Chem. Soc. **131** (47), 17270 (2009)
42. C.J. Delebecque, A.B. Lindner, P.A. Silver, F.A. Aldaye, Science **333**(6041), 470 (2011)
43. E. Bindewald, R. Hayes, Y.G. Yingling, W. Kasprzak, B.A. Shapiro, Nucleic Acid Res. **36** (suppl 1), D392 (2008)
44. A. Fire, S. Xu, M.K. Montgomery, S.A. Kostas, S.E. Driver, C.C. Mello, Nature **391**(6669), 806 (1998)
45. C. Wagner, C. Ehresmann, B. Ehresmann, C. Brunel, J. Biol. Chem. **279**(6), 4560 (2004)
46. E. Laurenti, I. Barde, S. Verp, S. Offner, A. Wilson, S. Quenneville, M. Wiznerowicz, H.R. MacDonald, D. Trono, A. Trumpp, Stem Cells **28**(8), 1390 (2010)
47. K.Y. Chang, I. Tinoco, PNAS **91**(18), 8705 (1994)
48. S. Hoeprich, Q. Zhou, S. Guo, D. Shu, G. Qi, Y. Wang, P. Guo, Gene Ther. **10**(15), 1258 (2003)
49. L. Ponchon, G. Beauvais, S. Nonin-Lecomte, F. Dardel, Nat. Protocols **4**(6), 947 (2009)
50. C. Chen, S. Sheng, Z. Shao, P. Guo, J. Biol. Chem. **275**(23), 17510 (2000)
51. S.T. Stern, S.E. McNeil, Toxicol. Sci. **101**(1), 4 (2008)
52. S. Singh, A. Sharma, G.P. Robertson, Cancer Res. **72**(22), 5663 (2012)
53. Y. Shu, M. Cinier, S.R. Fox, N. Ben-Johnathan, P. Guo, Mol. Ther. **19**(7), 1304 (2011)
54. J.B. Lee, J. Hong, D.K. Bonner, Z. Poon, P.T. Hammond, Nat. Mater. **11**(4), 316 (2012)
55. J.B. Bramsen, J. Kjems, Front Genet. **3**, 154 (2012)
56. R. Kanasty, J.R. Dorkin, A. Vegas, D. Anderson, Nat. Mater. **12**(11), 967 (2013)
57. X.D. Yang, D.R. Mahapatra, R.V.N. Melnik, in *AIP Conference Proceedings*, vol. 952 (AIP Publishing, 2007), pp. 229–237
58. S. Guo, N. Tschammer, S. Mohammed, P. Guo, Hum. Gene Ther. **16**(9), 1097 (2005)
59. A. Khaled, S. Guo, F. Li, P. Guo, Nano Lett. **5**(9), 1797 (2005)
60. J. Yano, K. Hirabayashi, S.I. Nakagawa, T. Yamaguchi, M. Nogawa, I. Kashimori, H. Naito, H. Kitagawa, K. Ishiyama, T. Ohgi, T. Irimura, Clin. Cancer Res. **10**(22), 7721 (2004)
61. H. Li, W.X. Li, S.W. Ding, Science **296**(5571), 1319 (2002)
62. C. Zhang, Curr. Opin. Mol. Ther. **11**(6), 641 (2009)
63. M.R. Fabian, N. Sonenberg, W. Filipowicz, Annu. Rev. Biochem. **79**(1), 351 (2010)
64. M. Paliy, R. Melnik, B.A. Shapiro, Phys. Biol. **6**(4), 046003 (2009)
65. S.R. Badu, R. Melnik, M. Paliy, S. Prabhakar, A. Sebetci, B.A. Shapiro, Eur. Biophys. J. **43** (10–11), 555 (2014)
66. T. Kim, B.A. Shapiro, J. Biomol. Struct. Dyn. **31**(5), 495 (2013)
67. J. Vieregg, W. Cheng, C. Bustamante, I. Tinoco, J. Am. Chem. Soc. **129**(48), 14966–14973 (2007)
68. M. Paliy, R. Melnik, B.A. Shapiro, Phys. Biol. **7**(3), 036001 (2010)
69. T. Hansson, C. Oostenbrink, W. van Gunsteren, Curr. Opin. Struct. Biol. **12**(2), 190 (2002)
70. W. van Gunsteren, D. Bakowies, R. Brgi, I. Chandrasekhar, M. Christen, X. Daura, P. Gee, A. Glttli, T. Hansson, C. Oostenbrink, C. Peter, J. Pitera, L. Schuler, T. Soares, H. Yu, CHIMIA Int. J. Chem. **55**(10), 856 (2001)
71. X. Wang, Y. Wang, L. Zheng, J. Chen, Curr. Med. Chem. **21**(17), 1968 (2014)
72. I.M. Moustafa, H. Shen, B. Morton, C.M. Colina, C.E. Cameron, J. Mol. Biol. **410**(1), 159 (2011)
73. N.J. Deng, P. Cieplak, Biophys. J. **98**(4), 627 (2010)
74. J.W. Chu, G.S. Ayton, S. Izvekov, G.A. Voth, Mol. Phys. **105**(2–3), 167 (2007)
75. J.W. Chu, S. Izveko, G.A. Voth, Mol. Simul. **32**(3–4), 211 (2006)
76. G.S. Ayton, W.G. Noid, G.A. Voth, Curr. Opin. Struct. Biol. **17**(2), 192 (2007)
77. J. Zhou, I.F. Thorpe, S. Izvekov, G.A. Voth, Biophys. J. **92**(12), 4289 (2007)
78. F. Ercolessi, J.B. Adams, Euro. Phys. Lett. **26**(8), 583 (1994)

79. M.S. Daw, M.I. Baskes, Phys. Rev. B **29**, 6443 (1984)
80. F. Ercolessi, E. Tosatti, M. Parrinello, Phys. Rev. Lett. **57**, 719 (1986)
81. G.S. Ayton, J.L. McWhirter, P. McMurtry, G.A. Voth, Biophys. J. **88**(6), 3855 (2005)
82. G.S. Ayton, G.A. Voth, Biophys. J. **87**(5), 3299 (2004)
83. G.S. Ayton, G.A. Voth, Int. J. Multiscale Comput. Eng. **2**(2), 291 (2004)
84. T.E. Ouldridge, A.A. Louis, J.P.K. Doye (2010)
85. F. Mathieu, S. Liao, J. Kopatsch, T. Wang, C. Mao, N.C. Seeman, Nano Lett. **5**(4), 661 (2005)
86. M. Bulacu, N. Goga, W. Zhao, G. Rossi, L. Monticelli, X. Periole, D.P. Tieleman, S.J. Marrink, J. Chem. Theory Comput. **9**(8), 3282 (2013)
87. I. Bahar, A. Rader, Curr. Opin. Struct. Biol. **15**(5), 586 (2005)
88. F. Tama, M. Valle, J. Frank, C.L. Brooks, PNAS **100**(16), 9319 (2003)
89. V. Tozzini, Curr. Opin. Struct. Biol. **15**(2), 144 (2005)
90. N. Hori, S. Takada, J. Chem. Theory Comput. **8**(9), 3384 (2012)
91. R. Das, D. Baker, PNAS **104**(37), 14664 (2007)
92. J. Bernauer, X. Huang, A.Y.L. Sim, M. Levitt, RNA **17**(6), 1066 (2011)
93. F. Ding, S. Sharma, P. Chalasani, V.V. Demidov, N.E. Broude, N.V. Dokholyan, RNA **14** (6), 1164 (2008)
94. J. Bida, R. Das, Curr. Opin. Struct. Biol. **22**(4), 457 (2012)
95. Z. Xia, D.P. Gardner, R.R. Gutell, P. Ren, J. Phys. Chem. B **114**(42), 13497 (2010)
96. J.C. Phillips, R. Braun, W. Wang, J. Gumbart, E. Tajkhorshid, E. Villa, C. Chipot, R. D. Skeel, L. Kal, K. Schulten, J. Comput. Chem. **26**(16), 1781 (2005)
97. D. MacKerell, D. Bashford, M. Bellott, R.L. Dunbrack, J.D. Evanseck, M.J. Field, S. Fischer, J. Gao, H. Guo, S. Ha, D. Joseph-McCarthy, L. Kuchnir, K. Kuczera, F.T.K. Lau, C. Mattos, S. Michnick, T. Ngo, D.T. Nguyen, B. Prodhom, W.E. Reiher, B. Roux, M. Schlenkrich, J.C. Smith, R. Stote, J. Straub, M. Watanabe, J. Wirkiewicz-Kuczera, D. Yin, M. Karplus, J. Phys. Chem. B **102**(18), 3586 (1998)
98. N. Foloppe, A.D. MacKerell Jr, J. Comput. Chem. **21**(2), 86 (2000)
99. A.D. MacKerell, N.K. Banavali, J. Comput. Chem. **21**(2), 105 (2000)
100. W. Humphrey, A. Dalke, K. Schulten, J. Mol. Graph. **14**(1), 33 (1996)
101. S.R. Badu, R. Melnik, M. Paliy, S. Prabhakar, A. Sebetci, B.A. Shapiro, in *Proceedings of IWBBIO-2014* (International Work-Conference on Bioinformatics and Biomedical Engineering, 2014), pp. 601–607
102. M. Zuker, Nucl. Acids Res. **31**(13), 3406 (2003)
103. N.R. Markham, M. Zuker, in *Bioinformatics*, ed. by J.M. Keith, no. 453 in Methods in Molecular Biology (Humana Press, 2008), pp. 3–31
104. Z. Bai, Appl. Numer. Math. **43**(12), 9 (2002)
105. P. Guo, O. Coban, N.M. Snead, J. Trebley, S. Hoeprich, S. Guo, Y. Shu, Adv. Drug Deliv. Rev. **62**(6), 650 (2010)